Supplement of Biogeosciences, 18, 25–38, 2021
https://doi.org/10.5194/bg-18-25-2021-supplement

Biogeosciences Open Access EGU

Supplement of

Southern Ocean Biogeochemical Argo detect under-ice phytoplankton growth before sea ice retreat

Mark Hague and Marcello Vichi

Correspondence to: Mark Hague (mark.hague@alumni.uct.ac.za)

Contents

1. Figures S1 to S10
2. Table 1

Additional Supporting Information

Figures S1-S4 provide additional examples to supplement Figure 3 in the paper. Figures for all time series analysed in this study can be provided on request. Panels in Figure S5 are identical to Figure 6 in the paper, but show the relation between sea ice concentration and phenology for the other 3 study regions in the Weddell and Bellinghausen/Amundsen Seas. Note that the marked early decrease in sea ice concentration shown in Figure S5B is due to the formation of an open ocean polynya associated with the Maud Rise seamount 2017 only (see **?**), all other years have concentrations above ∼90% until retreat in late November.

Table S1. Table of all floats used in this study, including both the WMO ID and MBARI ID (for identifying floats on the SOCCOM website). The years of data which where used are shown, although there may be more available data at the time of reading. Mean locations for each float are also shown based on the time interval used for calculations.

WMO ID / MBARI ID	Years Sampled	Mean Latitude	Mean Longitude
5904768 / 0570SOOCN	2016	64.8°S	166.7°W
5904671 / 0507SOOCN	2016 2017 2018	62.3°S	82°E
5905636 / 12754SOOC	2018	67°S	149.4°W
5905078 / 12371SOOC	2017	66.6°S	124.4°W
5904858 / 12551SOOC	2017 2018	73.9°S	148.7°W
5904184 / 9091SOOCN	2014	61.4°S	147.4°W
5904469 / 9096SOOCN	2018	60.4°S	23.2°E
5904767 / 0568SOOCN	2016 2018	63.2°S	145.5°W
5904859 / 12549SOOC	2017 2018	70.2°S	104.3°W
5904857 / 12381SOOC	2017 2018	72.8°S	167.2°W
5905100 / 12361SOOC	2017 2018	65.2°S	166.3°E
5904860 / 12541SOOC	2017 2018	72.1°S	164.8°W
5905075 / 8501SOOCN	2017 2018	68.9°S	102.8°W
5904472 / 9275SOOCN	2015 2016 2017 2018	68.5°S	25.9°W
5904855 / 12559SOOC	2017 2018	68.3°S	83.8°W
5905077 / 12379SOOC	2017	65.7°S	107.1°W
5904468 / 9099SOOCN	2015 2016 2017 2018	65°S	2.3°E
5904471 / 9094SOOCN	2015 2016 2017 2018	65.7°S	4°E
5904397 / 9125SOOCN	2015 2016 2017 2018	61.2°S	2.4°W
5905080 / 12366SOOC	2017	65°S	117.7°W

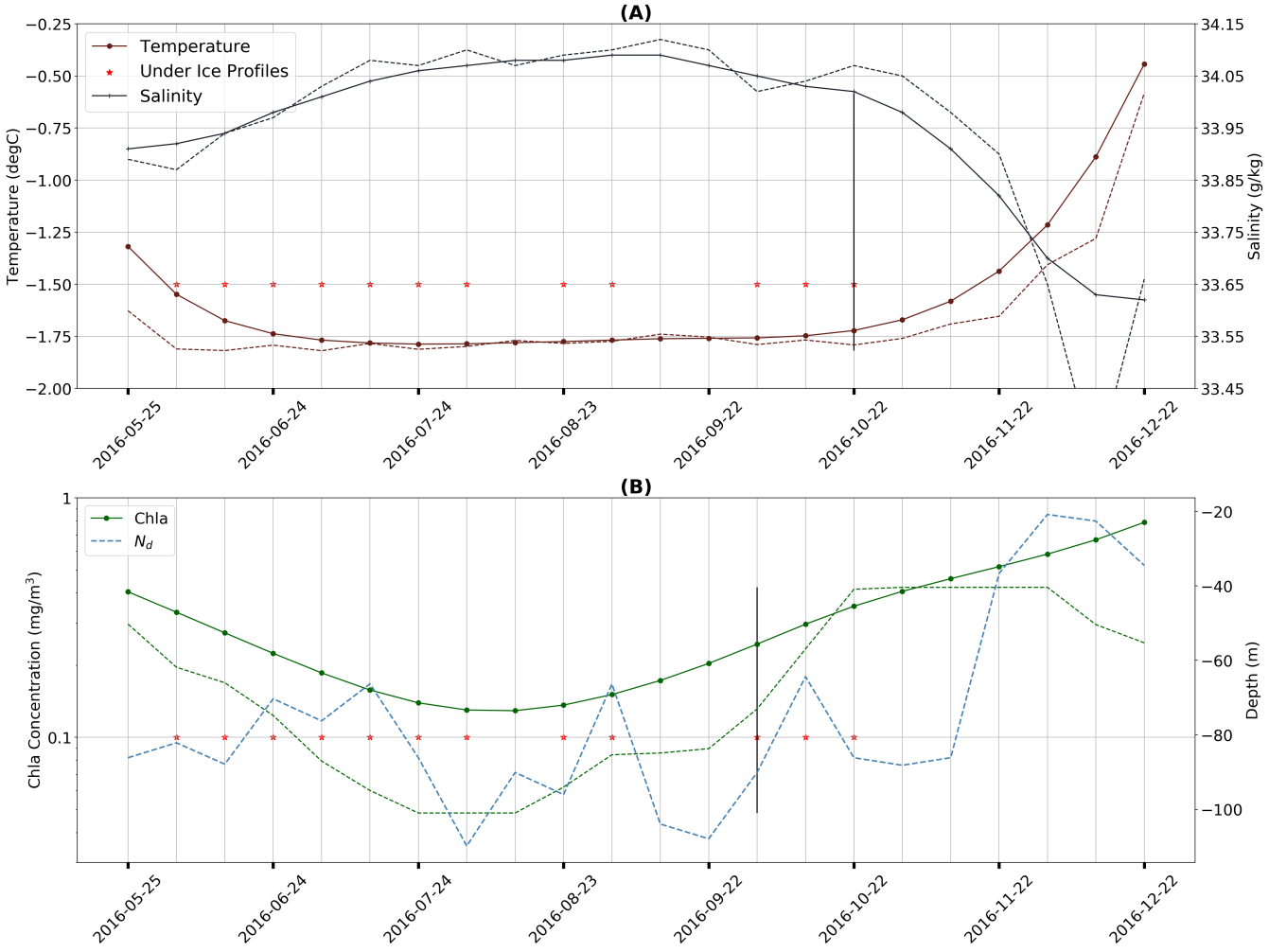

Figure S1. Additional time series of key properties as in Figure 3, but for a float in the Indian Ocean sector at ∼63°S in 2016.

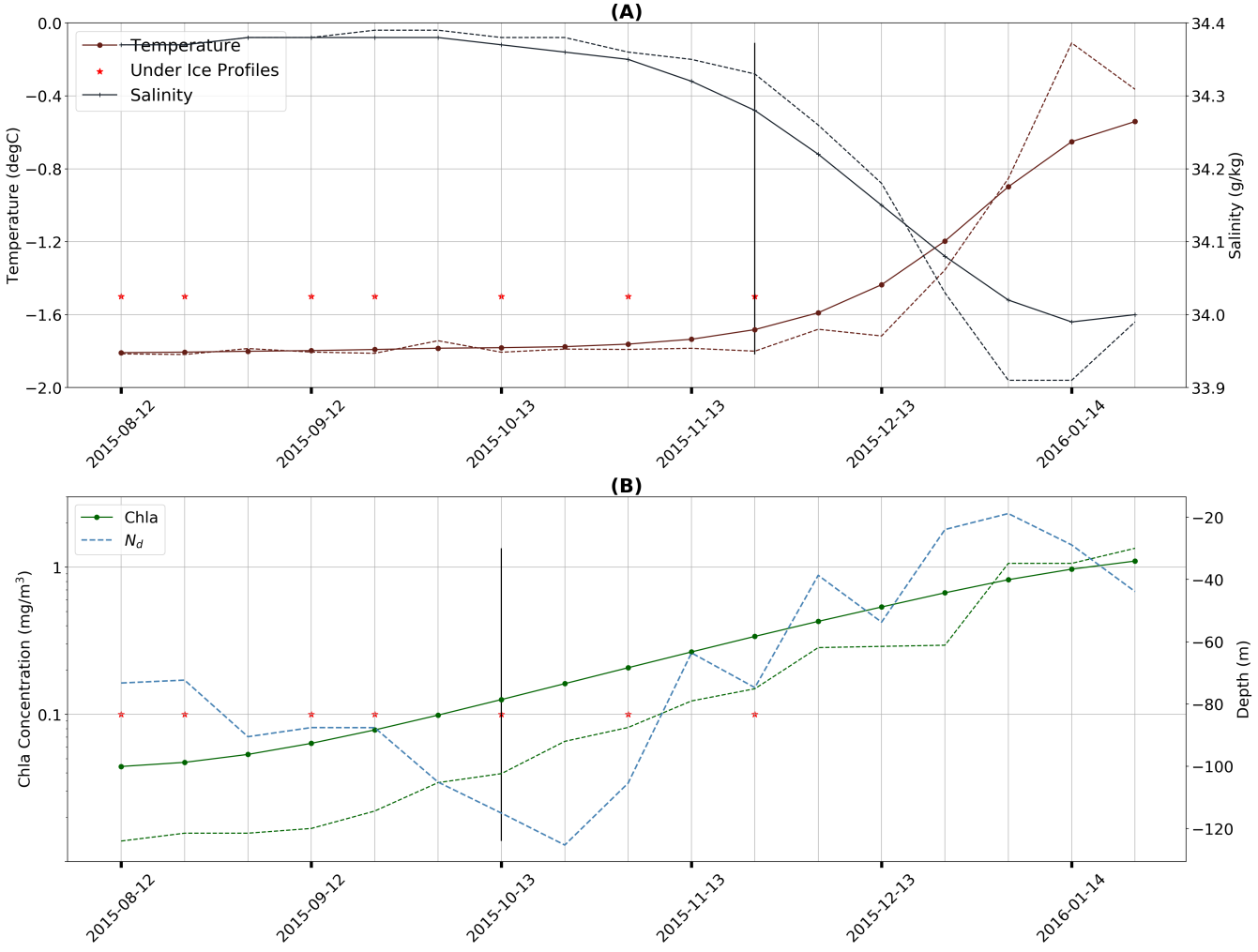

Figure S2. The same as above, but for a float in the western Weddell Sea ($\sim$ 40°W) at $\sim$68.5°S in 2015.

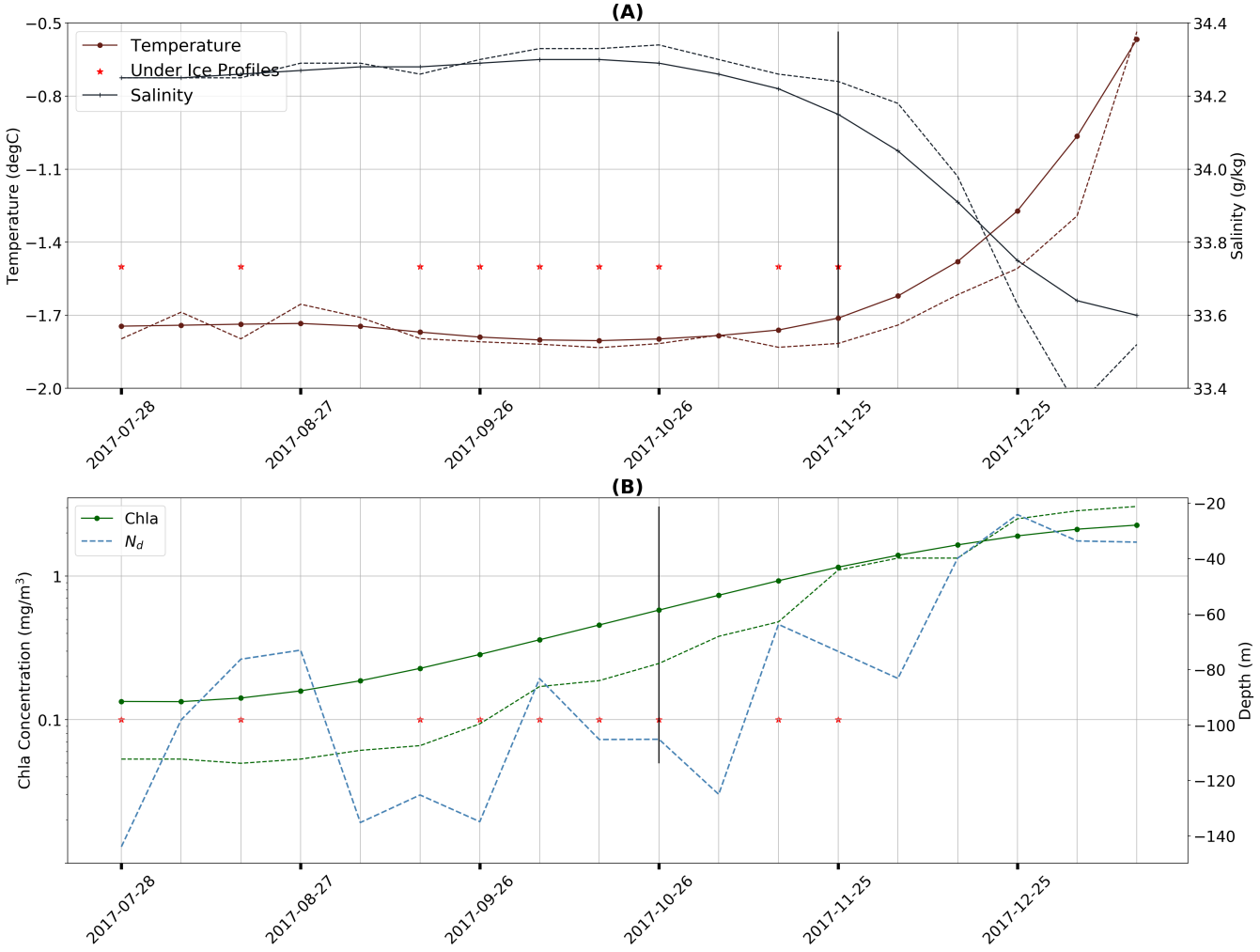

Figure S3. The same as above, but for a float north east of the Ross Sea at ∼65°S, ∼168°E in 2017.

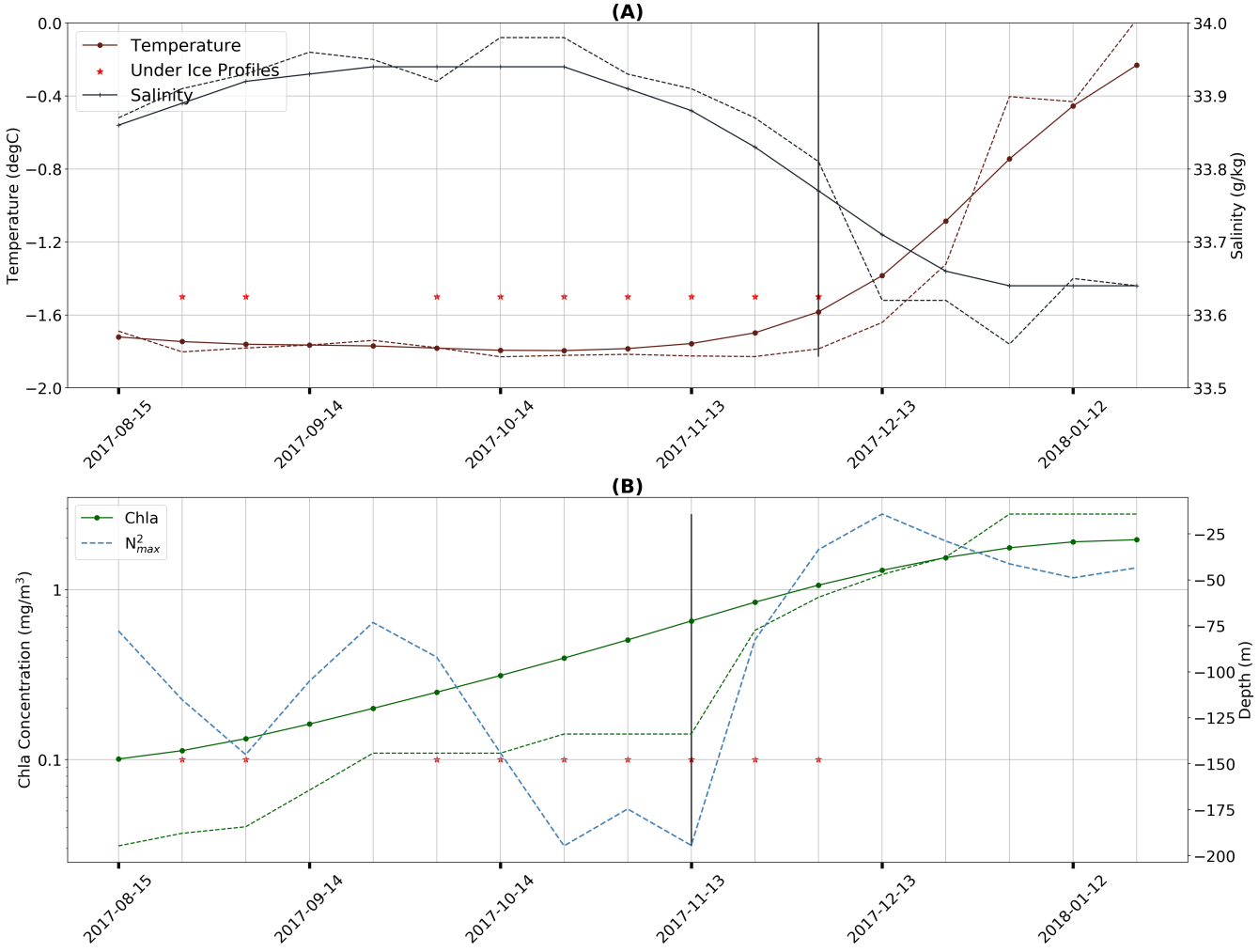

Figure S4. The same as above, but for a float in the Bellinghausen/Amundsen Sea at ∼68°S in 2017.

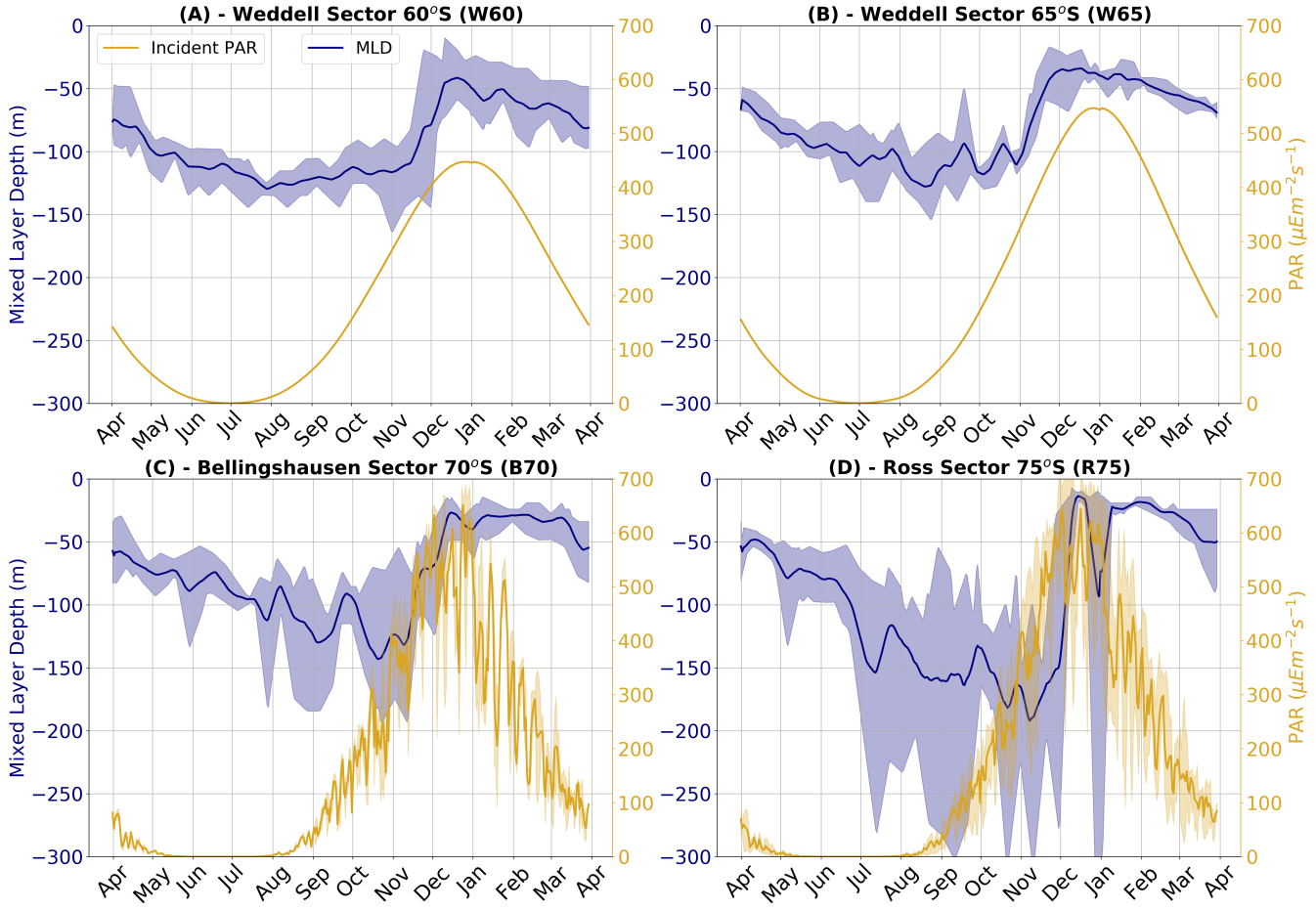

Figure S5. Time series of incident Photosynthetically Available Radiation (PAR; yellow curves) and mixed layer depth (as estimated by the stratification depth, N_d; blue curves) for each of the four study regions discussed in the text. Shading around each curve represents both the spatial and temporal variability present in each dataset as in Figure 6 in the main text.

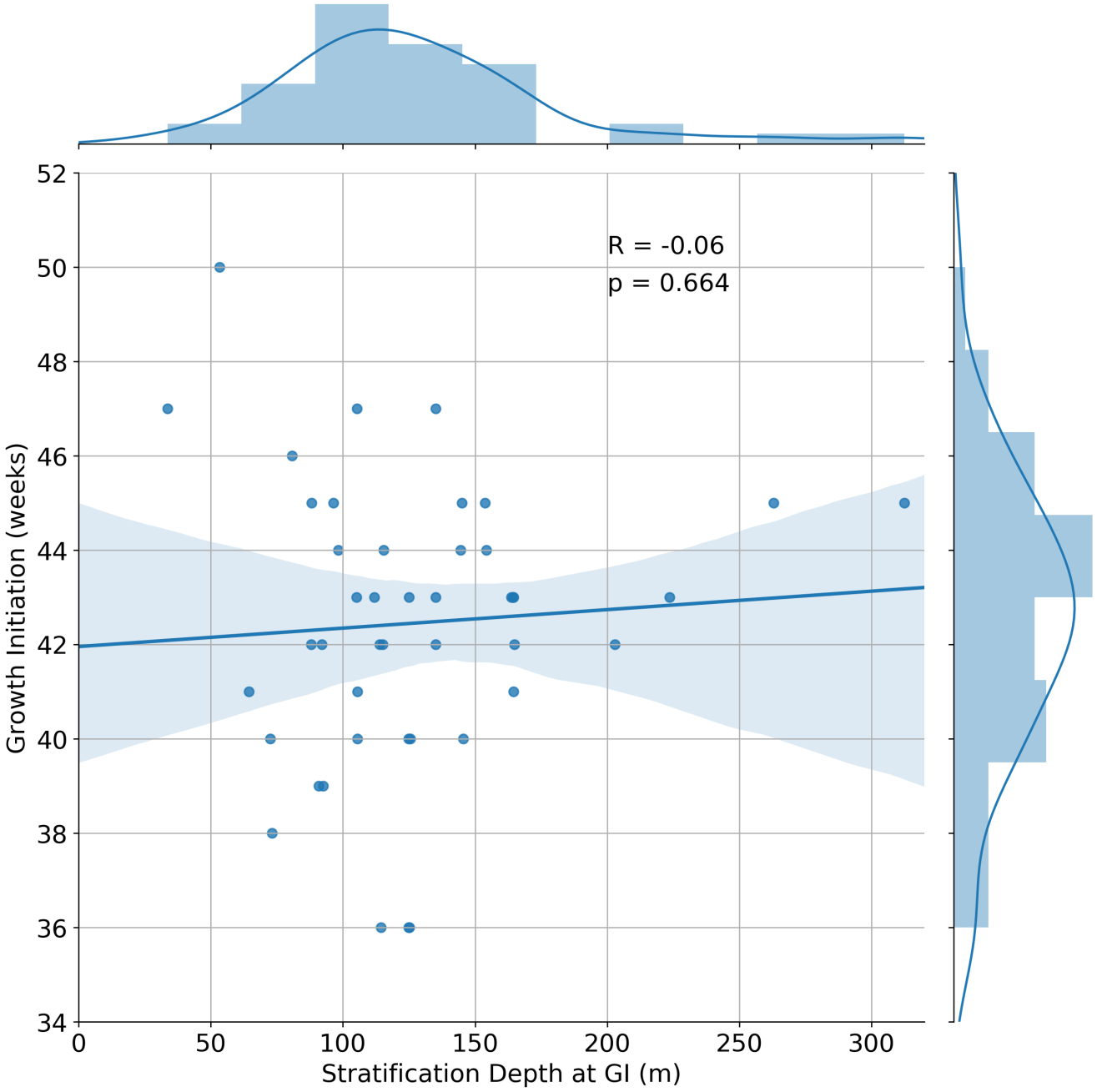

Figure S6. Stratification Depth at the timing of GI plotted against GI for each of the 44 melt events detected. Overlain in blue is the linear regression with the 95% confidence intervals for 1000 bootstrapped resamples shaded in light blue. Histograms and PDFs of each variable are shown along the edge of the axes.

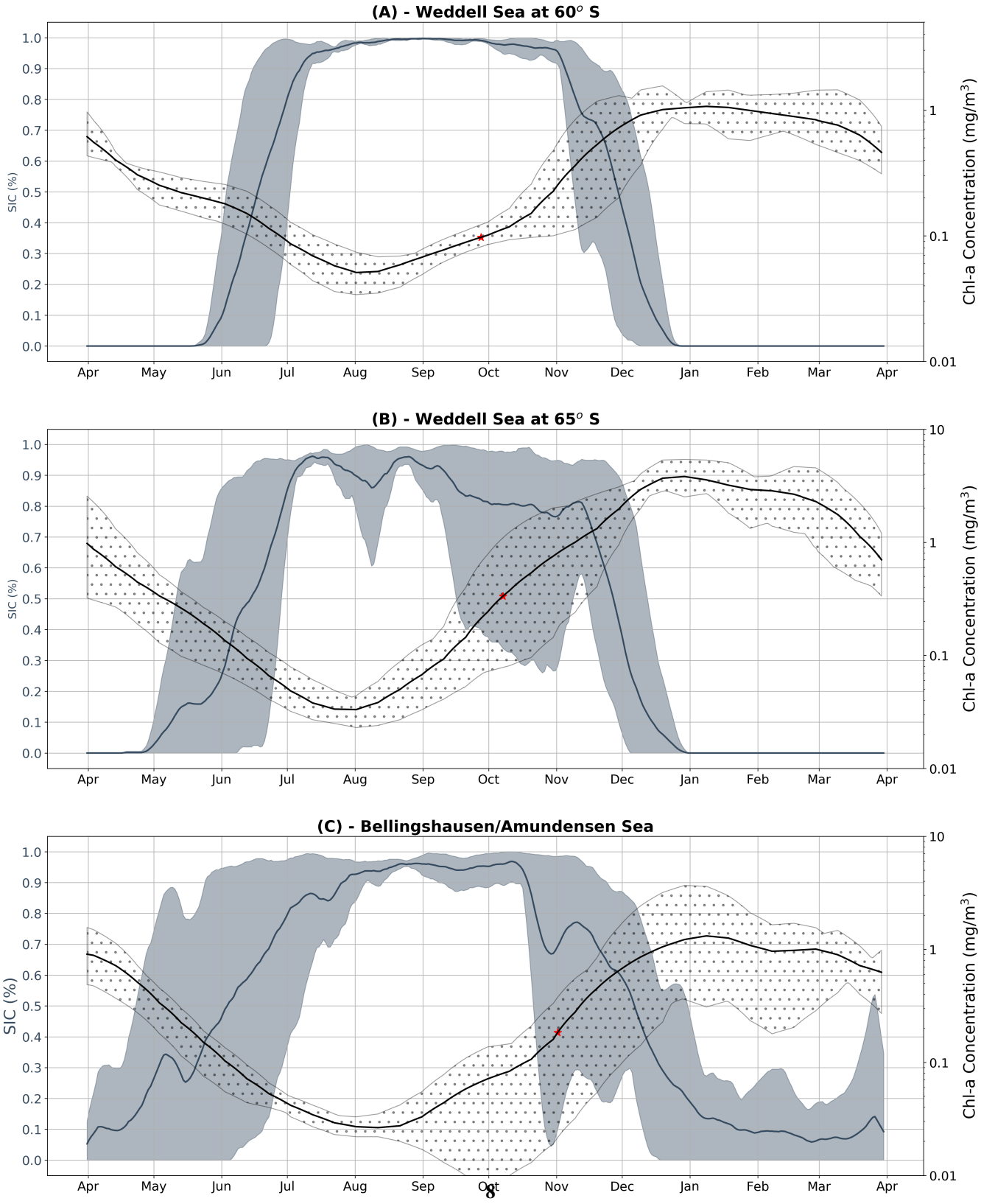

Figure S7. Time series of satellite sea ice concentration versus float mixed layer chl-a as in Figure 6, except for regions **(A)**: W60 , **(B)** W65 and **(C)**:B70.

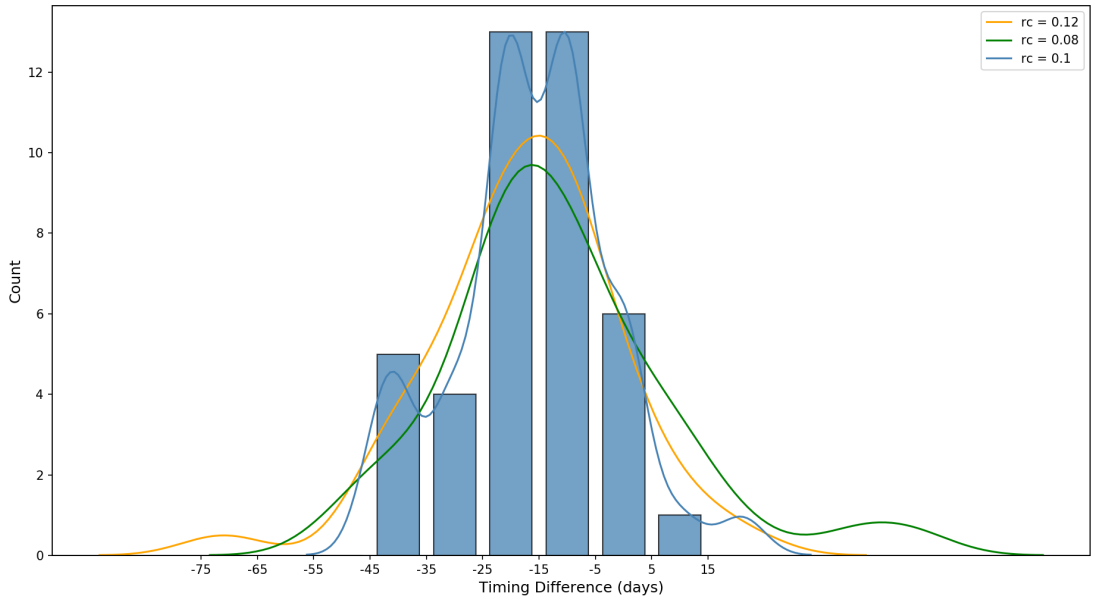

Figure S8. The same as Figure 5 in the paper, but with GI computed using the mean mixed layer POC rather than chl-a.

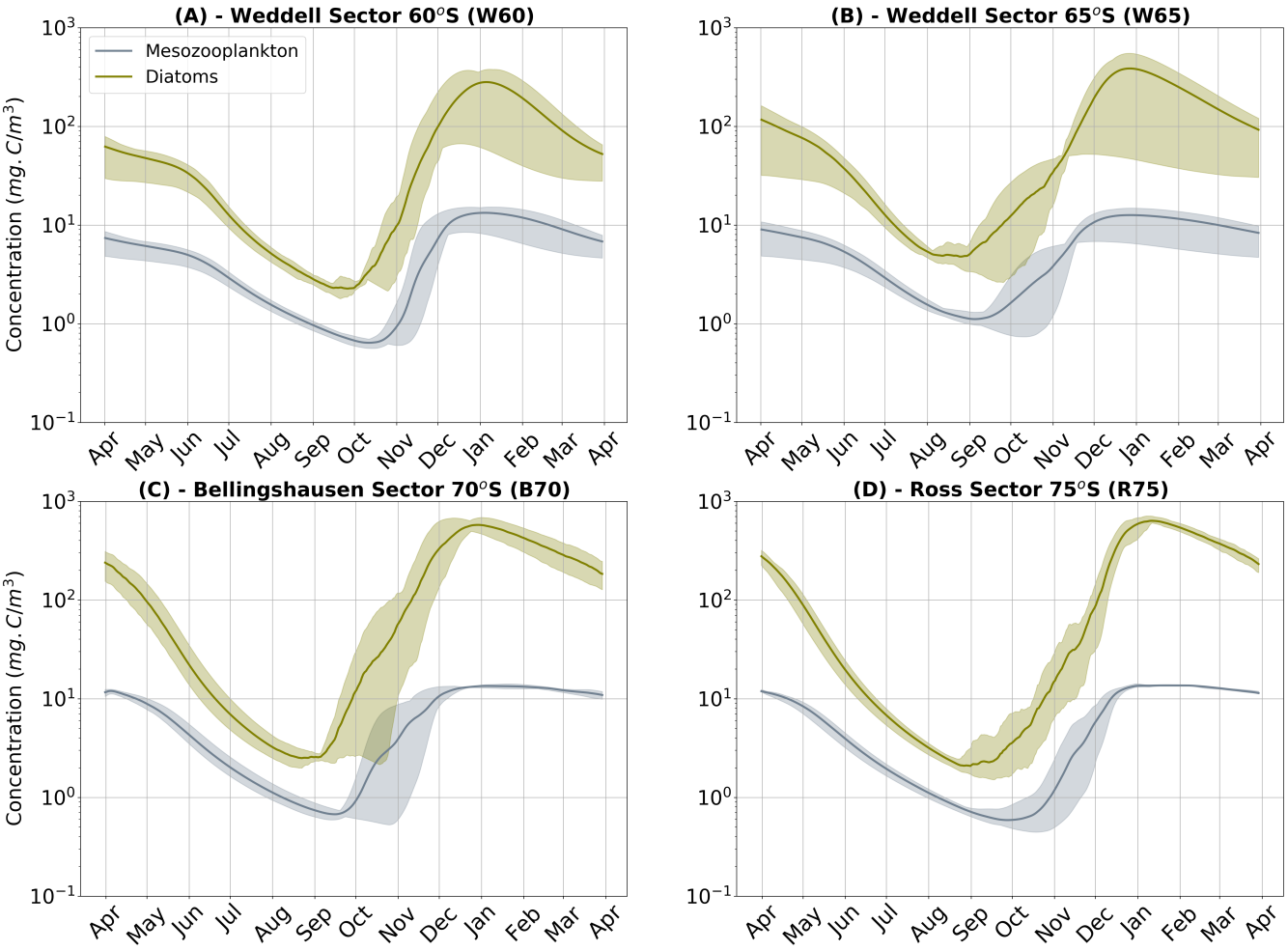

Figure S9. Time series of diatom and mesozooplankton concentrations for each study region for the LLA experiment. The other 2 core experiments show the same relationship. Shading around each curve represents both the spatial and temporal variability present in each dataset as in Figure 6 in the main text.

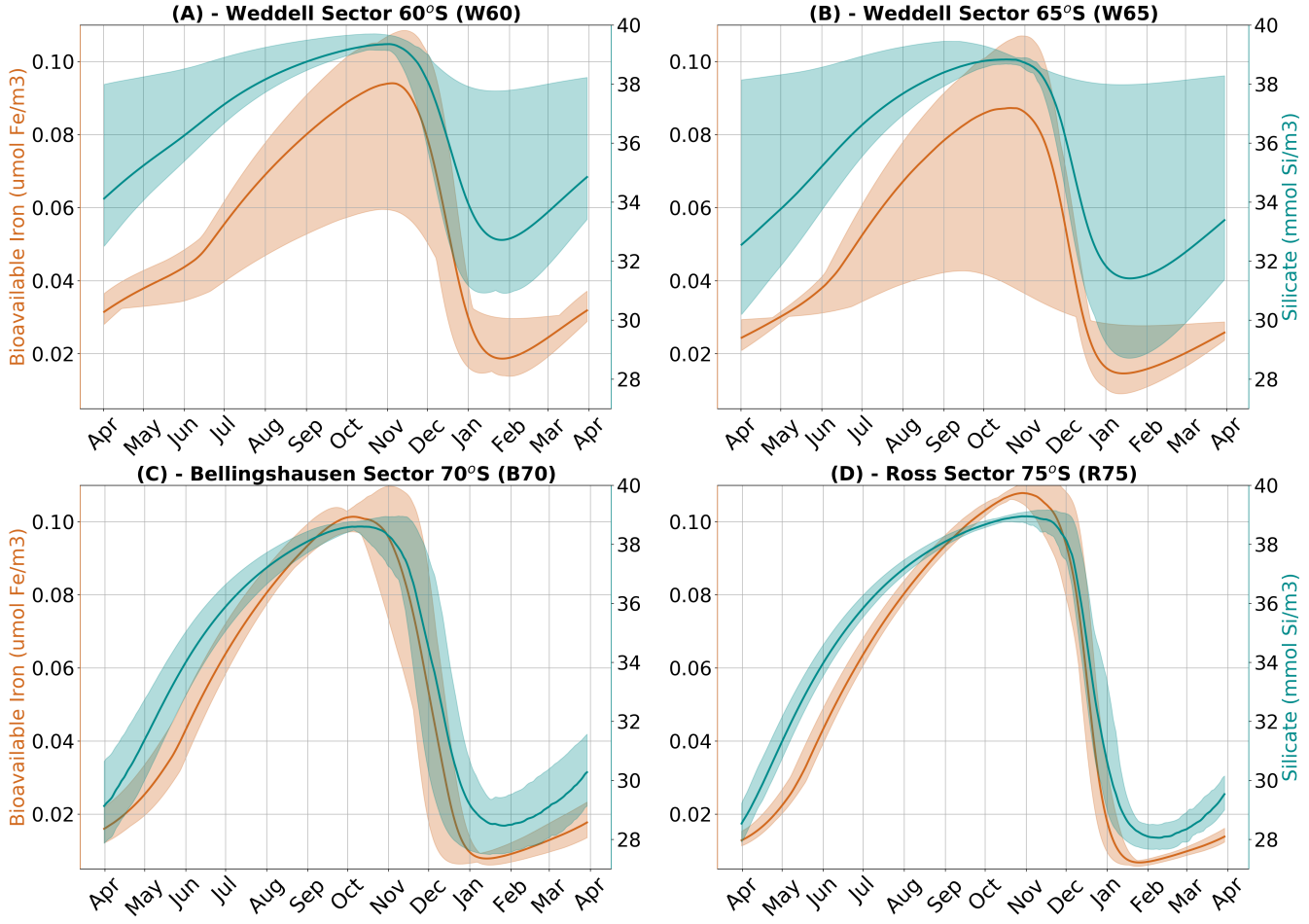

Figure S10. Time series of bioavailable iron (brown) and silicate (green) concentrations in each of the 4 study regions (only for the LLA experiment). Shading around each curve represents both the spatial and temporal variability present in each dataset as in Figure 6 in the main text.